SOCAR Proceedings

Drilling & Completion

journal home page: http://proceedings.socar.az

EFFECT OF DISPERSION STRENGTHENING ON THE PERFORMANCE OF $C_{DIAMOND}$–(WC–CO) COMPOSITE DRILLING TOOLS

B. T. Ratov[1], V. A. Mechnik[2], N. A. Bondarenko[2], A. B. Kalzhanova[3], V. A. Chishkala[4], Z. T. Matayeva[1], V. L. Khomenko*[5]

[1]*Kazakh National Research Technical University named after K. I. Satpayev, Almaty, Kazakhstan*

[2]*V. Bakul Institute for Superhard Materials of the National Academy of Sciences of Ukraine, Kyiv, Ukraine*

[3]*Caspian State University of Technology and Engineering named after Sh. Yesenov, Aktau, Kazakhstan*

[4]*V. N. Karazin Kharkiv National University, Kharkiv, Ukraine*

[5]*Dnipro University of Technology, Dnipro, Ukraine*

ABSTRACT

The study examines the effect of ZrO_2 micropowder additive (at 3 and 6 wt%) on the mechanical performance and wear behavior of $25C_{diamond}$–(70.5WC–4.5Co) composites fabricated by spark plasma sintering (SPS), as well as the performance of impregnated drill bits based on these composites during exploration drilling in Kazakhstan. It was found that introducing 3 wt% ZrO_2 into the $25C_{diamond}$–(70.5WC–4.5Co) composite reduces the wear rate by weight WR from $9.124\pm0.544\cdot10^{-5}$ to $4.116\pm0.382\cdot10^{-5}$ g/m, by volume WV from $9.237\pm0.645\cdot10^{-12}$ to $4.220\pm0.424\cdot10^{-12}$ m³/s, and the specific wear rate WS from $7.142\pm0.512\cdot10^{-13}$ to $4.022\pm0.254\cdot10^{-13}$ m³/(N·m). The twofold increase in wear resistance observed in the $25C_{diamond}$–(67.68WC–4.32Co)–$3ZrO_2$ composite compared to the base $25C_{diamond}$–(70.5WC–4.5Co) is attributed to grain refinement of WC, improved fracture toughness, and the transformation of the metastable tetragonal phase t-ZrO_2 into the thermodynamically stable monoclinic m-ZrO_2 phase. Even lower wear values were recorded for the $25C_{diamond}$–(64.86WC–4.14Co)–$6ZrO_2$ composite: WR = $2.107\pm0.204\cdot10^{-5}$ g/m, WV = $2.102\pm0.162\cdot10^{-12}$ m³/s, and WS = $1.724\pm0.118\cdot10^{-13}$ m³/(N·m), which is approximately 4.3 times lower than those of the base sample. The superior wear resistance of the 6% ZrO_2 composite is linked to a higher content of the monoclinic m-ZrO_2 phase, resulting from a more complete transformation of t-ZrO_2. Field tests showed that the drilling footage achieved by the impregnated core bit based on the $25C_{diamond}$–(64.86WC–4.14Co)–$6ZrO_2$ composite was four times greater than that of the standard core bit based on the $25C_{diamond}$–(70.5WC–4.5Co) mixture during exploration drilling by «KazakhmysBarlau» LLP.

Keywords: diamond core drill bit; composite; tungsten carbide; cobalt; zirconium dioxide; wear resistance; spark plasma sintering.

Date submitted: 25.08.2025 **Date accepted:** 12.12.2025

1. Introduction

The continuous development of the oil, gas, and mining industries in Kazakhstan and globally necessitates using drilling tools with enhanced mechanical and operational properties [1]. Correctly selected drilling mode parameters allow achieving maximum efficiency of their use [2, 3]. Impregnated diamond core drill bits are widely used to explore mineral deposits in medium- to soft-hardness rock formations [4]. Composite diamond-containing materials (CDCM) based on WC–Co matrices are broadly utilized in manufacturing a wide range of drilling tools, including impregnated diamond bits [5].

The physical, mechanical, and operational characteristics of CDCM in the $C_{diamond}$–(WC–Co) system depend on the phase composition, microstructure, and morphology, which are themselves determined by the properties of the components and the sintering methods and processing parameters employed [6–9]. However, during drilling of hard and abrasive rocks, the cemented carbide matrix of these materials is subjected to intense abrasive, fatigue, and adhesive wear, limiting their service life and reducing the performance of drill bits. Furthermore, weak adhesion between diamond particles and the matrix leads to diamond loss during operation, negatively impacting wear resistance [10]. Additional drawbacks include the brittleness of the carbide matrix [11], as well as deteriorated strength parameters (hardness, compressive and flexural strength, fracture toughness) and wear resistance under high contact loads, potentially resulting in total failure of the material [12].

Currently, $C_{diamond}$–(WC–Co) composites in impregnated drill bits do not ensure sufficient performance when drilling

**E-mail:* inteldriller@gmail.com

http://dx.doi.org/10.5510/OGP20260201193

hard and abrasive formations. Regardless of composition or sintering technique, CDCM must exhibit high strength and wear resistance [13, 14] and withstand elastic and plastic deformation [15]. Improving the mechanical and operational characteristics of $C_{diamond}$–(WC–Co) composites is thus a critical scientific and technical objective, as its resolution will significantly expand the applicability of impregnated diamond core drill bits.

Numerous studies have addressed the mechanical properties of these CDCM.

For example, [16] reported that coarse WC grains (>2 μm) cause spontaneous microcracking and insufficient mechanical performance, including low wear resistance. In [17], adding 0.5 wt% nano-Al_2O_3 to WC–8Co (produced by powder metallurgy) refined WC grains while increasing both hardness and fracture toughness. Nanostructured WC–Co composites were shown in [18] to outperform microstructured ones in hardness, toughness, and strength.

The influence of powder preparation and sintering temperature on WC–8Co properties was explored in [19], revealing that materials prepared via ultrasonic vibration and sintered at 1250 °C displayed homogeneous microstructures and improved mechanical performance. The influence of Co content on the microstructural features and mechanical behavior of ultrafine-grained WC–Co composites produced by spark plasma sintering (SPS) was studied in [20], showing that increasing Co content enhances density, fracture toughness, and bending strength, though at the cost of decreasing hardness. Optimal mechanical properties were achieved at 8% Co, with a hardness of 19.87 GPa, fracture toughness of 12.27 MPa·$m^{0.5}$, and flexural strength of 1834 MPa.

Thermal expansion behavior of WC–Co composites was examined via dilatometry and laser flash analysis in [21], indicating that the thermal expansion coefficient strongly depends on cobalt content. At the same time, WC grain size has little influence. In [22], correlations were found between flexural strength, hardness, and fracture toughness in powder metallurgy composites, with flexural strength initially increasing and then decreasing as hardness ranged from 800 to 1500 kg/mm^2. SPS-fabricated 94WC–6Co composites showed peak density (~99.6%) and Vickers hardness (~1400) at 1200 °C [23]. The tribological behavior of WC–Co under reciprocating friction was investigated in [13] as a function of Co content and WC particle size, revealing relationships between wear rate, friction coefficient, and testing conditions.

The wear performance of fine-grained WC–VC–Co composites under ball-on-disc tribometry with Ru and VC additions was analyzed in [14]. An inverse relationship between hardness and wear rate was found, with VC having a stronger effect on improving wear resistance than Ru.

In [15], WC grain sizes from 200 nm to 4.5 μm and Co contents from 3 to 24 % were evaluated for wear resistance under different loads. Results showed that under high loads, wear resistance improved with larger WC grain size and lower Co content, though hardness remained nearly constant. Fine-grained nanostructured materials showed lower wear resistance than coarse-grained ones due to reduced fracture toughness. Under low-load conditions, the wear rate decreased with smaller WC grain sizes and higher Co content. In [24], wear resistance of WC–Co and tool steels varied significantly with applied load (up to two orders of magnitude), but was less affected by sliding speed.

ZrO_2 is increasingly used as a strengthening additive in composites due to its excellent high-temperature properties such as fracture toughness, strength, hardness, corrosion resistance, and melting point [25]. ZrO_2 also exhibits transformation toughening due to a phase change from metastable tetragonal *t*-ZrO_2 to thermodynamically stable monoclinic *m*-ZrO_2. To stabilize *t*-ZrO_2 at room temperature, Y_2O_3 is often used [26]. Small additions of Y_2O_3 to WC–Co improve WC grain refinement, increasing hardness and fracture toughness [27].

In [28], the structure of $C_{diamond}$–(WC–Co)–ZrO_2 composites (grain size, diamond–matrix bonding, fracture patterns) formed by SPS was shown to depend strongly on ZrO_2 content. As shown in [29], adding 3% Y_2O_3-stabilized ZrO_2 to 25$C_{diamond}$–(70.5WC–4.5Co) improved mechanical properties and diamond retention. A 6% ZrO_2 addition increased relative density from 0.948 to 0.990, an increase in the flexural strength from 1935±80 to 2660±115 MPa, and an increase in fracture toughness from 13.8±0.71 to 16.9±0.76 MPa·$m^{0.5}$. The improvement in these parameters is achieved by refining the grains of the main WC phase and transforming the tetragonal *t*-ZrO_2 phase.

Tribological testing data on $C_{diamond}$–(WC–Co) diamond bits for hard rock drilling remains limited. An exception is [30], which investigated wear resistance of impregnated bits made from 25$C_{diamond}$–(70.5WC–4.5Co) and 25$C_{diamond}$–(68.62WC–4.38Co)–2ZrO_2, sintered at 20–1350 °C, 30 MPa for 3 minutes. Adding 2% ZrO_2 reduced the wear rate threefold during granite drilling. Wear resistance data obtained by nanoindentation on metal-matrix CDCM, though further validation is needed.

In summary, improving the wear resistance of these composites remains a key scientific and engineering challenge critical to developing more effective drilling tools for hard and abrasive formations. However, there is still limited data on fracture toughness and wear behavior of CDCM and tools made from them with varied ZrO_2 content. Additive concentration significantly affects essential material properties such as hardness, fracture toughness, ductility, and wear resistance. Targeted control of WC–Co–ZrO_2 and $C_{diamond}$–(WC–Co)–ZrO_2 composite properties through compositional and structural variation is possible, though nontrivial due to the multilayered nature of the resulting materials with differing thicknesses, phase compositions, and structures.

The purpose of this study is to comprehensively assess how dispersed ZrO_2 nanopowder additives affect the hardness and fracture toughness of WC–Co matrices, the wear resistance of $C_{diamond}$–(WC–Co) composites formed via spark plasma sintering, and the wear resistance of impregnated drill bits based on these materials during granite drilling.

2. Objects and methods of research

Sample sintering

The hard alloy matrix samples were fabricated from powder mixtures containing tungsten carbide (WC), cobalt (Co), and zirconium dioxide (ZrO_2). In contrast, the CDCM (composite diamond-containing materials) samples were made from the same base mixtures with the addition of diamond powder. To prepare the mixtures for spark plasma sintering (SPS) of composite samples with a diameter of 25 mm and thickness of 5 mm, the following powders were used: diamond powder (De Beers, South Africa) with

grit size 500/400 (average grain size 0.45 μm), tungsten carbide WC 1750 H (Global Tungsten & Powders spol. s.r.o., Bruntál, Czech Republic) with average particle size of 2.0–4.0 μm, cobalt powder (standard GOST 9721–79) with average particle size of 2.0–3.0 μm, and zirconium dioxide ZrO_2 partially stabilized with 3 wt% Y_2O_3 (NANOE, Ballainvilliers, France) with average particle size of 20–100 nm. The compositions of the initial mixtures used for sintering are presented in table 1.

Powder mixtures for the sintering of composites 94WC–6Co (Sample 1), 91.18WC–5.82Co–3ZrO_2 (Sample 2), and 88.36WC–5.64Co–6ZrO_2 (Sample 3) were mixed in a Pulverisette planetary mill (Fritsch) for 4 hours using 1.5 mm balls at an acceleration of 640 m/s². The resulting mixtures were dried in a furnace at 80 °C. The sintering of the hard alloy matrix samples (Samples 1–3) in the form of «pellets» (25 mm diameter, 5 mm thickness) was carried out in graphite dies using spark plasma sintering at a holding temperature of 1350 °C under a pressure of 30 MPa for 3 minutes [31]. The electric current was 5000 A, the voltage was 5 V, and the heating rate was 400 °C/min. Sintering was performed under vacuum (6 Pa). The temperature was measured with a CHINO IR-AH2 pyrometer directed on the surface of the graphite die. To avoid interaction between the die material and the sintered composite, the working surfaces of the dies were coated with boron nitride.

Due to the plasma effect, Spark plasma sintering enables extremely fast heating and a short sintering time. This feature helps avoid grain recrystallization and achieve equilibrium conditions, opening up possibilities for producing new materials, including CDCM with previously unattainable properties and nanocrystalline matrices.

The sintered composite samples were ground using a diamond grinding wheel (1A1-200×20×51 D213 (K50) G), and then polished on an ATM Saphir 550 automatic polishing machine using platinum and silver disks and diamond suspensions until a surface roughness of Ra < 0.1 μm was achieved by ISO 4287. Images of the polished surfaces of the sintered composite samples for hardness and fracture toughness testing are shown in figure 1. As seen in the figure, all polished surfaces exhibit a mirror-like appearance, which is essential for conducting experimental investigations.

Table 1
Compositions of initial powder mixtures for sample sintering, wt%

Sample	$C_{diamond}$	WC	Co	ZrO_2
1	–	94	6	–
2	–	91.18	5.82	3
3	–	88.36	5.64	6
4	25	70.5	4.5	–
5	25	67.68	4.32	3
6	25	64.86	4.14	6

Powder mixtures for sintering CDCM samples 4–6 were prepared using the following procedure. First, the required amounts of non-diamond powders (table 1) were mixed in a Pulverisette planetary mill (Fritsch) for 4 hours using 1.5 mm balls at an acceleration of 640 m/s². The mixtures were then dried in an oven at 80 °C. Afterward, the required amount of diamond powder was added to the dried mixtures, mixed in an alcohol medium until a homogeneous mixture was obtained, and then dried again in a drying cabinet. Sintering of the CDCM samples was carried out in graphite dies using the same spark plasma sintering parameters as for Samples 1–3. Microstructural images of the sintered CDCM samples (Samples 4–6) are shown in figure 2.

As shown in figure 2, the described method for preparing diamond-containing mixtures followed by spark plasma sintering allows the formation of CDCM samples with a uniform distribution of diamond grains within the hard alloy matrix, which is critical for developing efficient drilling tools.

Microstructural analysis method

The morphology and microstructure of the sintered samples were studied using scanning electron microscopy (SEM) with a ZEISS EVO 50 XVP electron microscope (Zeiss, Germany) equipped with an Ultim Max 100 (Oxford Instruments, UK) energy-dispersive X-ray spectroscopy

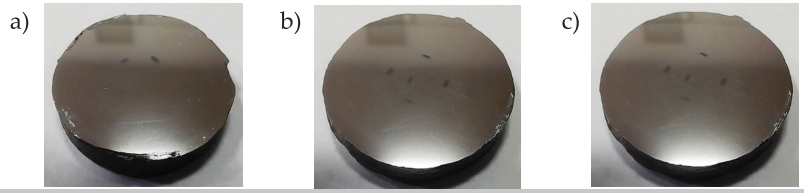

Fig. 1. Photographs of polished surfaces of sintered hard alloy matrix samples:

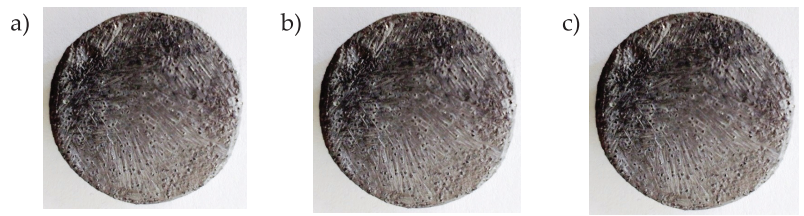

Fig. 2. Photographs of sintered CDCM samples

(EDS) analyzer. For each sample, at least twenty micrographs were obtained. Image processing was performed using the «ImageJ» software package to determine grain boundaries and construct grain size distribution histograms [32]. The images were pre-calibrated for scale, then automated processing was performed in ImageJ using adaptive threshold segmentation and a grain separation algorithm. Equivalent grain diameters were calculated from the segmented regions, and distribution histograms were constructed; mean values and standard deviations were used to assess statistical significance. This refinement improves the transparency of the quantitative portion of the microstructural analysis.

Fracture toughness measurement method

A FALCON 500 microhardness tester (Innovatest, Netherlands) was used at a 100 N load to determine Vickers hardness and visualize indentations and radial cracks. It was equipped with a digital microscope with a 5-megapixel matrix. Hardness and fracture toughness values were calculated using the tester's licensed «IMPRESSIONS» software, enabling semi-automatic mechanical properties acquisition.

The hardness value was calculated using the following formula:

$$H_v = 463.6\frac{F}{d_{av}^2}$$

where F is the load applied to the indenter, N; $d_{av}=(d_1+d_2)/4$ is half of the average diagonal length of the indentation, μm.

The fracture toughness K_{Ic} of the composite was determined by [33] using the following expression:

$$\frac{K_{Ic}\Phi}{Hd_{av}^{0.5}} = 0.15k\left(\frac{C_{av}}{d_{av}}\right)^{-1.5}$$

where Φ is the constraint factor (≈3), HV is the Vickers hardness, $C_{av}=(C_1+C_2)/4$ is the average length of radial cracks measured from the center of the indentation, and k=3.2. The value of k was determined empirically using K_{Ic} values measured by standard methods on macroscale specimens.

By combining the expression for calculating Vickers hardness with the Evans and Charles equation, the final formula for determining fracture toughness takes the form

$$K_{Ic} = 74.2\cdot 10^{-2}\frac{F}{C_{av}^{1.5}}$$

The errors in determining HV and K_{Ic} were calculated as the standard deviations from the mean values.

Method for determining the wear resistance of sintered CADM specimens

The wear behavior of sintered composite abrasive diamond material (CADM) specimens was investigated using a «cylinder–shaft» scheme by turning a cylindrical core of Korostyshev granite (Ukraine, Zhytomyr region), rock drillability category X, with a test stand based on the IA616 engine lathe (fig. 3). Wear resistance tests were carried out at a spindle speed of 400 rpm, a depth of cut per pass of 0.5 mm, a cross feed of 0.5 mm/rev, a longitudinal feed of 0.13 mm/rev, and a normal load of 10 N. The length of the cutting part of the granite core was 200 mm, and its initial diameter was 70 mm. The weight loss of each CADM specimen was measured after 10 passes with a total cutting time of 3300 s (a single pass being 200 mm long and lasting 230 s). Technical water was used as the cooling fluid.

The microrelief of the friction surface of the CADM specimens after tribological testing was analyzed using an Axioscope 5 optical microscope (Zeiss, Germany).

Based on the measured mass loss, the wear rate of sintered CADM specimens was evaluated using the following tribological characteristics.

The weight wear rate W_R was calculated by the mass loss ΔW over the friction path L:

$$W_R = \frac{\Delta W}{L}$$

The volumetric wear rate W_V was determined as follows:

$$W_V = \frac{\Delta V}{t}$$

The specific wear rate W_S was defined as the volume loss per unit path length and applied normal load P [34]:

$$W_S = \frac{\Delta V}{LP}$$

where $\Delta V = \frac{m_1 - m_2}{\rho}$, with m_1 and m_2 being the mass of the specimen before and after wear testing, g; L is the total sliding distance, m.

The sliding distance L was calculated as:

$$L = \frac{\pi Dnt}{60}$$

where D is the core diameter, m; n is the spindle speed, rpm; t is the test duration, s.

Weighing was performed before and after experiments

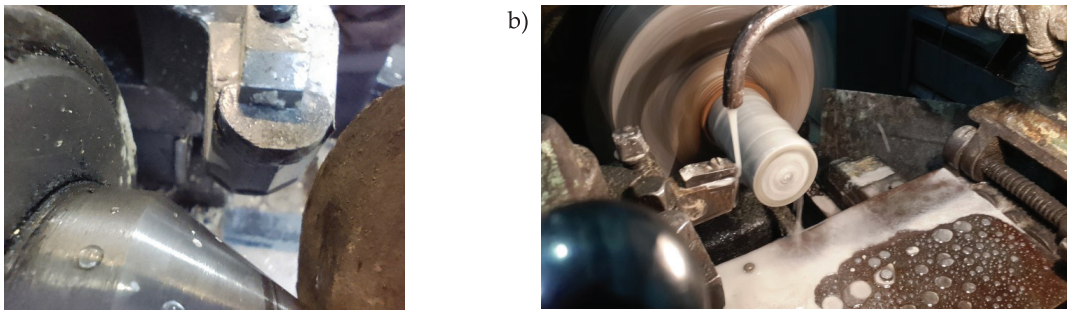

a) image of the CADM insert and granite core mounting

b) image of the wear testing process

Fig. 3. Test bench for evaluating the wear resistance of sintered CADM specimens

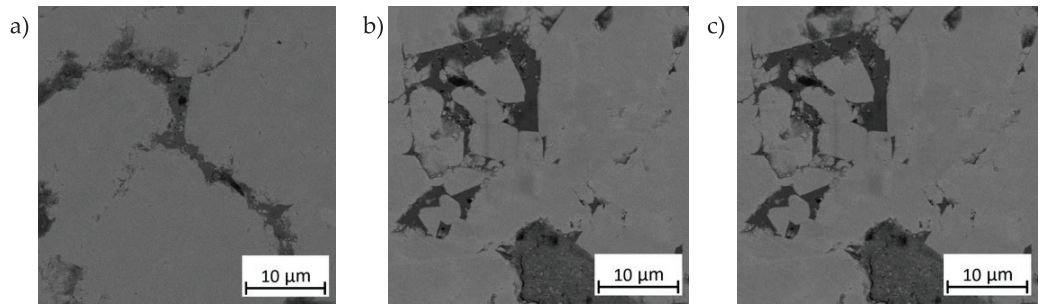

a) 94WC–6Co (sample 1); b) 91.18WC–5.82Co–3ZrO_2 (sample 2); c) 88.36WC–5.64Co–6ZrO_2 (sample 3).

Fig. 4. SEM images of microstructure areas of sintered composite samples

using AXIS AD 200 analytical balances. All tests were conducted under normal atmospheric conditions and 40% relative humidity. The test procedure complies with international standards ASTM G99-959, DIN 50324, and ISO 20808 [35, 36].

3. Research results and discussion

Microstructure of sintered samples

Figure 4 presents typical microstructures of sintered composite samples 1–3 obtained by scanning electron microscopy in material contrast mode (fig. 4a–c). A dense, uniform tungsten carbide (WC) matrix is observed in all investigated samples, forming the composite material's main phase. In these images, WC has the highest brightness due to the highest atomic number of W among all system components. Analysis of the microstructural images demonstrates clearly defined boundaries between WC grains and the cobalt (Co) binder phase. In figure 4, cobalt has the darkest contrast, corresponding to its lower atomic number.

In samples 2 and 3, containing 3 and 6 % stabilized zirconium dioxide (ZrO_2), gray inclusions sized 4–10 μm are clearly visible on the polished surfaces. These particles mostly have rounded or irregular morphology and stand against the matrix background. The agglomeration of primary smaller nanoparticles formed by them has a higher atomic number than cobalt, and accordingly appears as light gray areas that are somewhat darker than WC grains.

The choice of ZrO_2 concentrations (3 and 6 % by weight) is based on literature data and preliminary laboratory tests, which demonstrated that this range achieves a compromise between pronounced strengthening and an acceptable reduction in matrix hardness. A concentration of 3% allows for the initial effect of dispersion strengthening to be observed, while 6% demonstrates the limit of the positive effect on fracture toughness and tribological properties without significant degradation of strength parameters. The text clarifies that further increases in the ZrO_2 content require separate study due to the risk of agglomeration and pore formation.

Grain size measurement results demonstrate that in sintered composites containing zirconium dioxide additives (samples 2 and 3), compared to the composite without zirconium dioxide (sample 1), a stable decrease in the average carbide grain size is achieved. All this can influence the physico-mechanical properties of the sintered composites.

The presented microstructural images indicate effective sintering with uniform phase distribution. ZrO_2 particles are well integrated into the carbide matrix, potentially contributing to the material's transformation and strengthening.

Mechanical properties of sintered samples

Values of hardness H_V (measured by Vickers indentation) and fracture toughness K_{Ic} of composites 94WC–6Co (sample 1), 91.18WC–5.82Co–3ZrO_2 (sample 2), and 88.36WC–5.64Co–6ZrO_2 (sample 3) are given in table 2. The maximum hardness HV (16.12±0.32 GPa) was recorded for the 94WC–6Co sample (sample 1). Adding 3% ZrO_2 to the 94WC–6Co composition (sample 2) led to a slight decrease in hardness H_V (from 16.12±0.32 to 15.64±0.40 GPa). H_V decreases slightly with further increase of ZrO_2 content in the 94WC–6Co composite (sample 3). At the same time, the hardness of samples 2 and 3 is almost equal, and the range of indenter penetration depth was the same. The decrease of H_V in samples 2 and 3 compared to sample 1 is caused by the influence of the ZrO_2 additive, whose hardness is less than that of WC. Lower H_V values in samples 2 and 3 compared to sample 1 can also be related to agglomeration of ZrO_2 particles and formation of nanopores near them.

In contrast, introducing ZrO_2 into the composite at concentrations $C_{ZrO_2} \leq 6\%$ positively affects fracture toughness. While there is a slight (~3%) decrease in hardness H_V, a more significant (up to 20%) increase in fracture toughness K_{Ic} of the composite sample is observed. For example, at zirco-

Table 2

Results of hardness H_V and fracture toughness K_{Ic} determination

Parameter	Sample		
	94WC–6Co (sample 1)	**91.18WC–5.82Co–3ZrO_2 (sample 2)**	**88.36WC–5.64Co–6ZrO_2 (sample 3)**
H_V, GPa	16.12±0.32	15.64±0.40	15.41±0.32
K_{Ic}, MPa·m$^{0.5}$	14.34±0.64	16.84±0.78	17.88±0.80

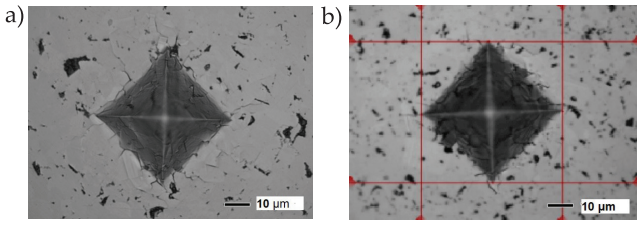

Fig. 5. Microphotographs of indenter imprints at C_{ZrO_2}=0 (a) and 3% (b)

nium dioxide concentration C_{ZrO_2}=6%, fracture toughness K_{Ic}=17.88±0.80 MPa·m$^{0.5}$, whereas at zirconium dioxide concentration C_{ZrO_2}=0 wt.%, fracture toughness K_{Ic}=14.34±0.64 MPa·m$^{0.5}$. Figures 5a and b show microphotographs of Vickers pyramid indents formed in composites 1 and 2 with ZrO_2 content of 0 and 3 %, respectively.

It is seen (fig. 5a) that in composite 1, inside the area of the Vickers pyramid imprint and around it, many cracks of significant size are observed. Such a family of cracks in sample 1 indicates excessive brittleness of the WC–6Co composite in the absence of zirconium dioxide. Whereas in composite 2 with 3 % zirconium dioxide content, significantly fewer cracks are observed (fig. 5b), and their length is also significantly less than in composite 1.

The non-monotonic dependence of the composite strength on ZrO_2 content is attributed to the combined effects of dispersion strengthening and modifications in structure and phase composition.

It should be noted that the efficiency of the dispersion strengthening mechanism increases with increasing C_{ZrO_2}, but the maximum fracture toughness is achieved at C_{ZrO_2}=6%. This increase in fracture toughness of this composite may correspond to changes in phase composition after sintering and forming the final structure.

Wear resistance of sintered CADM samples

Wear resistance testing of CADM samples also showed significant changes in properties caused by the physical nature and structure. Table 3 presents the results of wear rate determination for the studied CADM samples (samples 4–6, table 1). Experiments showed that fabricated sample 4 (C_{ZrO_2}=0%) under the technological conditions described above is characterized by wear rates by weight W_R (9.124±0.544·10^{-5} g/m), wear rates by volume W_V (9.237±0.645·10^{-12} m^3/s), and specific wear rate W_S (7.142±0.512·10^{-13} m^3/(N·m)). After introduction of zirconium dioxide ZrO_2 additive at 3%, the values of wear rates by weight W_R, volume W_V, and specific wear rate W_S decrease (from 9.124±0.544·10^{-5} g/m to 4.116±0.382·10^{-5} g/m, from 9.237±0.645·10^{-12} m^3/s to 4.220±0.424·10^{-12} m^3/s, and from 7.142±0.512·10^{-13} m^3/(N·m) to 4.022±0.254·10^{-13} m^3/(N·m), respectively). As can be seen from the obtained data, wear rates by weight W_R, volume W_V, and specific wear rate W_S for sample 5 are approximately 2 times lower than those for sample 4.

Reduction in wear rate of sample 25$C_{diamond}$–(67.68WC–4.32Co)–3ZrO_2 compared to sample 25$C_{diamond}$–(70.5WC–4.5Co) is attributed to the presence of zirconium dioxide, which allowed grain refinement of WC (fig. 4) along with a simultaneous increase in fracture toughness (table 2). With a further increase in zirconium dioxide content from 3 to 6% in the composite, a decrease in wear rate by weight W_R (from 4.116±0.382·10^{-5} g/m to 2.107±0.204×10^{-5} g/m), wear rate by volume W_V (from 4.220±0.424·10^{-12} m^3/s to 2.102±0.162×10^{-12} m^3/s), and specific wear rate W_S (from 4.022±0.254·10^{-13} m^3/(N·m) to 1.724±0.118·10^{-13} m^3/(N·m)) was observed, which is approximately 4.3 times lower than that of sample 4.

The decrease in wear rates W_R, W_V, and W_S in sample 25$C_{diamond}$–(64.86WC–4.14Co)–6ZrO_2 compared to sample 25$C_{diamond}$–(67.68WC–4.32Co)–3ZrO_2 is explained by its higher content of monoclinic phase *m*-ZrO_2 (a larger amount of

Table 3

CADM sample compositions and their tribological characteristics

Sample	Wear rate by weight W_R, 10^{-5} g/m	Wear rate by volume W_V, 10^{-12} m^3/s	Specific wear rate W_S, 10^{-13} m^3/(N·m)
25$C_{diamond}$–(70.5WC–4.5Co) (sample 4)	9.124±0.544	9.237±0.645	7.142±0.512
25$C_{diamond}$–(67.68WC–4.32Co)–3ZrO_2 (sample 5)	4.116±0.382	4.220±0.424	4.022±0.254
25$C_{diamond}$–(64.86WC–4.14Co)–6ZrO_2 (sample 6)	2.107±0.204	2.102±0.162	1.724±0.118

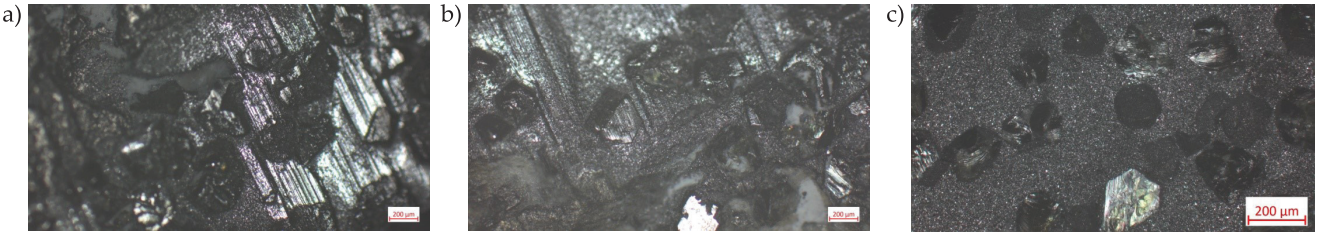

a) 25$C_{diamond}$–(70.5WC–4.5Co) (sample 4); b) 25$C_{diamond}$–(67.68WC–4.32Co)–3ZrO_2 (sample 5); c) 25$C_{diamond}$–(64.86WC–4.14Co)–6ZrO_2 (sample 6)

Fig. 6. Optical images of CADM microstructure areas after wear resistance testing, obtained in polarized light

tetragonal phase *t*-ZrO_2 transformed into thermodynamically stable monoclinic phase *m*-ZrO_2). Consequently, the wear rate obtained for sample 6 is significantly lower than for samples 4 and 5, confirming the higher structural perfection of the densely packed *m*-ZrO_2 phase. It can be considered that the wear rate is mainly determined by the amount of ZrO_2 additive, as well as the morphology and size of the phase constituents in the samples.

The above results indicate that the wear rates by weight W_R, volume W_V, and specific wear rate W_S have the lowest values at a zirconium dioxide concentration of C_{ZrO_2}=6%. This, in turn, indicates that the composite $25C_{diamond}$–(64.86WC–4.14Co)–$6ZrO_2$ is advisable for manufacturing tools for drilling hard and abrasive rocks.

Tribological tests of the studied CADM samples resulted in intensive abrasion of the hard alloy matrix and detachment of diamond grains. Figure 6 shows optical images of microstructure areas of samples $25C_{diamond}$–(70.5WC–4.5Co) (sample 4), $25C_{diamond}$–(67.68WC–4.32Co)–$3ZrO_2$ (sample 5), and $25C_{diamond}$–(64.86WC–4.14Co)–$6ZrO_2$ (sample 6), illustrating the features of diamond grain bonding strength with the hard alloy matrix. Analysis of figure 6a shows that in the selected area of sample $25C_{diamond}$–(70.5WC–4.5Co) (sample 4 without ZrO_2 additive), after wear resistance testing under the described conditions, a significant number of diamond grains detached from the hard alloy matrix are observed (pits from which diamond grains have fallen out). The formation of deep and wide grooves (scratches) on the working surface of sample 4 (fig. 6a) indicates strong abrasive wear of the hard alloy matrix due to penetration of rock particles and wear products into the soft (cobalt) phase.

In the selected area of sample $25C_{diamond}$–(67.68WC–4.32Co)–$3ZrO_2$ (sample 5), compared to sample $25C_{diamond}$–(70.5WC–4.5Co), significantly fewer diamond grains detached from the hard alloy matrix are observed (fig. 6b). Moreover, the friction surface of this sample shows finer and more evenly distributed scratches, and the worn surface is smoother.

Addition of 6% ZrO_2 micropowder to the CADM $25C_{diamond}$–(70.5WC–4.5Co) composition provides stronger bonding of diamond grains with the hard alloy matrix than in sample $25C_{diamond}$–(67.68WC–4.32Co)–$3ZrO_2$ (sample 5), which contains less ZrO_2 micropowder additive. In this case, no areas with diamond grain detachment are observed on the surface of sample $25C_{diamond}$–(64.86WC–4.14Co)–$6ZrO_2$ (fig. 6c).

Improved diamond grain retention in the matrix with the addition of ZrO_2 is not due to direct chemical adhesion, but to indirect effects: increased fracture toughness and a reduced rate of abrasive wear of the carbide matrix reduce the formation of deep pits and cavities from which grains fall out. Furthermore, the refinement of WC grains and a more uniform phase distribution increase the diamond-matrix contact density, further stabilizing the grains in the working surface. These mechanisms together ensure increased performance of drill bits in field tests.

Thus, it is experimentally confirmed that the addition of 3 and 6 % zirconium dioxide micropowder to the composite $25C_{diamond}$–(70.5WC–4.5Co) and the application of spark plasma sintering are promising for the production of drilling tools with enhanced mechanical properties.

Performance Characteristics of Diamond-Impregnated Drill Bits

Below are the results of industrial testing of experimental three core drill bits KSB-3M (bits 1–3), developed based on diamond-containing mixtures for CADM samples 4–6. The cutting part of core bit 1 was made using the diamond-containing mixture for CADM 4; core bit 2 was developed based on the diamond-containing mixture for CADM 5; and core bit 3 was developed based on the diamond-containing mixture for CADM 6. Photographs of the bits are shown in figure 7.

Geometric characteristics of the bits:

- Outer diameter – 95.6 mm;
- Inner diameter – 63.5 mm;
- Height of diamond-containing layer – 18 mm;
- Number of turns of the helical surface hosting diamond and non-diamond layers – 3;
- Pitch of the triple-start helical surface – 1 mm.

Tests were conducted during drilling of exploration wells at the geological site of «KazakhmysBarlau» LLP. Drilling was performed using the UKB-6S drilling rig. Wells were drilled with an initial inclination angle of 67°. The rock formations consist of coal-siliceous meta-argillites of dark gray color of VII–VIII hardness categories and chlorite-siliceous meta-phyllitic meta-aluvrolites of VII–X categories. Table 4 presents the results of industrial tests of drill bits.

Tests showed that the penetration of core drill bit 3, manufactured based on the diamond-containing mixture $25C_{diamond}$–(64.86WC–4.14Co)–$6ZrO_2$, exceeds the penetration of core bit 1, manufactured using the standard diamond-containing mixture $25C_{diamond}$–(70.5WC–4.5Co), by 4 times. Moreover, the developed diamond core bit 3 provides reliable operation throughout the entire service life without visible chipping of the diamond-containing layer. No areas of spalling of the hard alloy matrix near diamond grains or cracks, and no detachment of the diamond-containing layer from the core bit body, were detected on the cutting surface of the core bit. It should be noted that the results of industrial tests during well drilling with developed core bits 1–3 correlate with the wear rate results for sintered CADM samples 4–6 (tables 4 and 3).

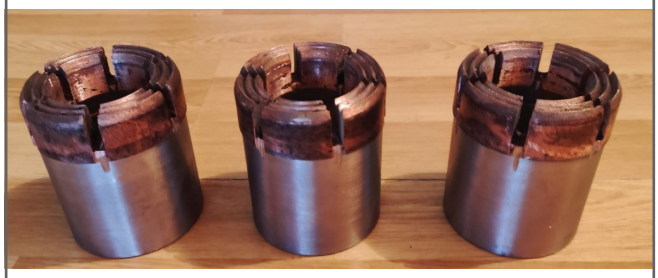

1 2 3

Fig. 7. Photographs of core drill bits

Table 4
Results of industrial tests of drill bits

Core bit	Well	Drilling interval, m	Penetration, m
1	S3-43	320-367	47
2	S-61 BA	104.6-195.8	91.2
3	S-50	44.6-240.2	195.6

The results of the conducted industrial tests demonstrate the quality of the developed composite diamond-containing materials and the competitiveness of drill bits manufactured based on them. The developed composites and tools are advisable for drilling hard and abrasive rock formations in geological exploration.

Conclusions

This work presents the results of studying the combined influence of the dispersion-strengthening additive of ZrO_2 nanopowder on the structure, mechanical properties, and wear behavior of CADM $25C_{diamond}$–(70.5WC–4.5Co) fabricated by SPS, and the operational characteristics of impregnated drill bits made based on them under drilling conditions. The nature and effectiveness of this influence depend on the concentration of ZrO_2.

1. Improving the wear resistance of the KAMs under consideration is a key objective, directly impacting the performance of drilling tools in hard and abrasive formations. Literary data on the fracture toughness and wear resistance of KAMs with varying ZrO_2 contents are limited, while the additive concentration significantly determines the material's performance properties.
2. Addition of ZrO_2 to the CADM composite $25C_{diamond}$–(70.5WC–4.5Co) in amounts of 3 and 6 % is accompanied by formation of a finer-grained hard alloy matrix structure with uniform distribution of components, including diamond grains, and an increase in fracture toughness from 14.34±0.64 to 16.84±0.78 MPa·$m^{0.5}$ and from 16.84±0.78 to 17.88±0.80 MPa·$m^{0.5}$, respectively.
3. Addition of 3% ZrO_2 to the CADM composite $25C_{diamond}$–(70.5WC–4.5Co) leads to reduction of wear rates by weight W_R from 9.124±0.544·10^{-5} to 4.116±0.382·10^{-5} g/m, by volume W_V from 9.237±0.645·10^{-12} to 4.220±0.424·10^{-12} m^3/s, and specific wear rate W_S from 7.142±0.512·10^{-13} to 4.022±0.254·10^{-13} m^3/(N·m). The wear rates W_R, W_V, and W_S for composite $25C_{diamond}$–(64.86WC–4.14Co)–6ZrO_2 have the lowest values of 2.107±0.204·10^{-5} g/m, 2.102±0.162·10^{-12} m^3/s, and 1.724±0.118·10^{-13} m^3/(N·m), respectively, which is approximately 4.3 times lower than for sample $25C_{diamond}$–(70.5WC–4.5Co).
4. The twofold increase in wear resistance of composite $25C_{diamond}$–(67.68WC–4.32Co)–3ZrO_2 compared to $25C_{diamond}$–(70.5WC–4.5Co) is due to the presence of ZrO_2, which allowed grain refinement of WC with simultaneous increase in fracture toughness, diamond retention, and phase transition of the tetragonal phase *t*-ZrO_2 (metastable at room temperature) to thermodynamically stable monoclinic phase *m*-ZrO_2. The improved wear resistance of composite $25C_{diamond}$–(64.86WC–4.14Co)–6ZrO_2 compared to $25C_{diamond}$–(67.68WC–4.32Co)–3ZrO_2 is explained by its higher content of monoclinic phase *m*-ZrO_2 (a larger amount of tetragonal *t*-ZrO_2 phase transformed to thermodynamically stable monoclinic *m*-ZrO_2).
5. Penetration of the impregnated core bit made from diamond-containing mixture $25C_{diamond}$–(64.86WC–4.14Co)–6ZrO_2 during exploration drilling at the geological site of «KazakhmysBarlau» LLP exceeds penetration of the impregnated core bit made from standard diamond-containing mixture $25C_{diamond}$–(70.5WC–4.5Co) by 4 times.
6. The results obtained interest the development of CADM sintering technology and its use in designing efficient impregnated diamond bits for geological exploration drilling of hard and abrasive rock formations.

The study was supported by the Science Committee of the Ministry of Science and Higher Education of the Republic of Kazakhstan (grant No. AP23484450) and V. Bakul Institute for Superhard Materials of the National Academy of Sciences of Ukraine.

References

1. Efendiyev, G. M., Mammadov, P. Z., Piriverdiyev, I. A., Sarbopeyeva, M. D. (2017). Selection of the best combination of bit types and technological parameters during drilling, taking into account uncertainty. *Procedia Computer Science*, 120, 67–74.

2. Pashchenko, O., Ratov, B., Khomenko, V., et al. (2024). Methodology for optimizing drill bit performance. *International Multidisciplinary Scientific GeoConference Surveying Geology and Mining Ecology Management, SGEM*, 24(1.1), 623–631.

3. Akhmetov, S. M., Efendiev, G., Akhmetov, N. M., et al. (2021). Investigation of the influence of the mode parameters of the drilling wells on the bit speed indicators. *News of the National Academy of Sciences of the Republic of Kazakhstan, Series of Geology and Technical Sciences*, 6(450), 37–45.

4. Song, D., Ren, Z., Yang, Y., et al. (2022). Drilling performance analysis of impregnated micro bit. *Mechanical Sciences*, 13(2), 867–875.

5. He, M., Li, N., Zhu, J., Chen, Y. (2020). Advanced prediction for field strength parameters of rock using drilling operational data from impregnated diamond bit. *Journal of Petroleum Science and Engineering*, 187, 106847.

6. Ratov, B. T., Mechnik, V. A., Bondarenko, M. O., Kolodnitskyi, V. M. (2022). Physical and mechanical properties of WC–Co–CrB_2 matrices of composite diamond-containing materials sintered by vacuum hot pressing for drilling tool applications. *Journal of Superhard Materials*, 44(4), 240–251.

7. Wang, X., Hwang, K. S., Koopman, M., et al. (2013). Mechanical properties and wear resistance of functionally graded WC-Co. *International Journal of Refractory Metals and Hard Materials*, 36, 46–51.

8. Tarragó, J. M., Roa, J. J., Valle, V., et al. (2015). Fracture and fatigue behavior of WC-Co and WC-CoNi cemented carbides. *International Journal of Refractory Metals and Hard Materials*, 49(1), 184–191.

9. Pero, R., Maizza, G., Montanari, R., Ohmura, T. (2020). Nano-indentation properties of tungsten carbide-cobalt composites as a function of tungsten carbide crystal orientation. *Materials*, 13(9), 2137.

10. Seal, M. (1963). The effect of surface orientation on the graphitization of diamond. *Physica Status Solidi* (b), 3(4), 658–664.

11. Ratov, B. T., Mechnik, V. A., Bondarenko, N. A., et al. (2024). Increasing the durability of an impregnated diamond core bit for drilling hard rocks. *SOCAR Proceedings*, 1, 24–31.

12. Ratov, B. T., Mechnik, V. A., Khomenko, V. L., et al. (2024). Influence of disperse-hardening additive chrome diboride on the structure of carbide matrixes of PDC drill bits. *Naukovyi Visnyk Natsionalnoho Hirnychoho Universytetu*, 4, 27–34.

13. Bonny, K., de Baets, P., Perez, Y., (2010). Friction and wear characteristics of WC-Co cemented carbides in dry reciprocating sliding contact. *Wear*, 268(11–12), 1504–1517.

14. Chipise, L., Jain, P. K., Cornish, L. A. (2021). Sliding wear characteristics of WC-VC-Co alloys with various Ru additions. *International Journal of Refractory Metals and Hard Materials*, 95, 105429.

15. Konyashin, I., Ries, B. (2014). Wear damage of cemented carbides with different combinations of WC mean grain size and Co content. Part I: ASTM wear tests. *International Journal of Refractory Metals and Hard Materials*, 46, 12–19.

16. Su, W., Zou, J., Sun, L. (2020). Effects of nano-alumina on mechanical properties and wear resistance of WC-8Co cemented carbide by spark plasma sintering. *International Journal of Refractory Metals and Hard Materials*, 92, 105337.

17. Sirota, V. V, Gevorkyan, É. S., Kovaleva, M. G., Ivanisenko, V. V. (2013). Structure and properties of nanoporous ceramic Al2O3 obtained by isostatic pressing. *Glass and Ceramics*, 69(9–10), 342–345.

18. Zhao, S., Song, X., Zhang, J., Liu, X. (2008). Effects of scale combination and contact condition of raw powders on SPS sintered near-nanocrystalline WC-Co alloy. *Materials Science and Engineering: A*, 473(1–2), 323–329.

19. Wang, B., Wang, Z., Yin, Z., et al. (2019). Effects of powder preparation and sintering temperature on consolidation of ultrafine WC-8Co tool material produced by spark plasma sintering. *Ceramics International*, 45(16), 19737–19746.

20. Liu, K., Wang, Z., Yin, Z., (2018). Effect of Co content on microstructure and mechanical properties of ultrafine grained WC-Co cemented carbide sintered by spark plasma sintering. *Ceramics International*, 44(15), 18711–18718.

21. Wang, H., Webb, T., Bitler, J. W. (2015). Study of thermal expansion and thermal conductivity of cemented WC-Co composite. *International Journal of Refractory Metals and Hard Materials*, 49(1), 170–177.

22. Fang, Z. Z. (2005). Correlation of transverse rupture strength of WC-Co with hardness. *International Journal of Refractory Metals and Hard Materials*, 23(2), 119–127.

23. Zhu, L, Liu, K., Li, Z. (2011). Study on the hardening and toughening mechanisms of WC–Co cemented carbides with plate-like WC grains. *Rare Metal Materials and Engineering*, 40, 443–446.

24. Gant, A. J., Gee, M. G. (2001). Wear of tungsten carbide-cobalt hardmetals and hot isostatically pressed high speed steels under dry abrasive conditions. *Wear*, 250–251(Part 2), 908–915.

25. Hannink, R. H. J., Kelly, P. M., Muddle, B. C. (2000). Transformation toughening in zirconia-containing ceramics. *Journal of the American Ceramic Society*, 83(3), 461–487.

26. Gaillard, Y., Jiménez-Piqué, E., Soldera, F., et al. (2008). Quantification of hydrothermal degradation in zirconia by nanoindentation. *Acta Materialia*, 56(16), 4206–4216.

27. Yang, Y., Luo, L.-M., Zan, X., et al. (2020). Synthesis of Y_2O_3-doped WC-Co powders by wet chemical method and its effect on the properties of WC-Co cemented carbide alloy. *International Journal of Refractory Metals and Hard Materials*, 92, 105324.

28. Mechnik, V. A., Rucki, M., Ratov, B. T., et al. (2022). Structure of $C_{diamond}$–(WC–6Co)–ZrO_2 composites formed by electrical plasma spark sintering. *Journal of Superhard Materials*, 44(5), 301–322.

29. Ratov, B. T., Mechnik, V. A., Rucki, M., et al. (2023). $C_{diamond}$–(WC–Co)–ZrO_2 Composite materials with improved mechanical and adhesive properties. *Journal of Superhard Materials*, 45(2), 103–117.

30. Ratov, B. T., Mechnik, V. A., Gevorkyan, E. S., et al. (2024). Investigating the wear resistance of $C_{diamond}$–(WC–Co)–ZrO_2 composite impregnated crowns in granite drilling. *Journal of Superhard Materials*, 46(4), 314–321.

31. Kodash, V. Y., Gevorkian, E. S. (2003). Tungsten carbide cutting tool materials. *USA Patent 6617271.*

32. Schneider, C. A., Rasband, W. S., Eliceiri, K. W. (2012). NIH Image to ImageJ: 25 years of image analysis. *Nature Methods*, 9(7), 671–675.

33. Evans, A. G., Charles, E. A. (1976). Fracture toughness determinations by indentation. *Journal of the American Ceramic Society*, 59(7–8), 371–372.

34. Fuertes, V., Cabrera, M. J., Seores, J., et al. (2019). Enhanced wear resistance of engineered glass-ceramic by nanostructured self-lubrication. *Materials and Design*, 168, 107623.

35. ASTM G99-17. (2017). Standard test method for wear testing with a pin-on-disk apparatus. *United States: ASTM.*

36. ASTM G171-03. (2017). Standard test method for scratch hardness of materials using a diamond stylus. *United States: ASTM.*